Role of the Binder in Mitigating Salt Deposition in 100cm2 Membrane Electrode Assembly CO2 Electrolyzers

ADVANCED ENERGY & SUSTAINABILITY RESEARCH
www.advenergysustres.com

Role of the Binder in Mitigating Salt Deposition in 100 cm^2 Membrane Electrode Assembly CO_2 Electrolyzers

Laura Gatti, Sara Verhovez, Alessio Mezza, Marco Etzi, Stefano Stassi, Candido F. Pirri, and Adriano Sacco**

The electrochemical reduction of carbon dioxide offers a promising approach to reduce CO_2 emissions while producing valuable chemicals. To date, CO production in membrane electrode assembly (MEA) electrolyzers employing anion exchange membranes results as the most industrially viable setup. However, industrial applicability of this technology is limited by the salt precipitation problem that compromises long-term operation. In this study, we first systematically optimized key electrode components using a 5 cm^2 commercial cell and then validated the results in 25 and 100 cm^2 electrolyzer under ambient conditions. Among the investigated parameters, the polymeric binder emerges as a critical element influencing both selectivity and stability, due to its impact on salt accumulation. In the 100 cm^2 electrolyzer, long-term electrochemical measurements conducted at industrially relevant current density (300 mA cm^{-2}) demonstrate significantly greater stability with PiperION−based cathodes, which maintained faradaic efficiency toward CO larger than 80% for 40 h operations, while Sustainion-based electrodes show a 60% drop after just 20 h. Cross-sectional elemental mapping confirms a direct correlation between the ionomeric binder and Cs salt accumulation in the electrode. This work provides valuable insight into mitigating salt formation and enhancing electrode longevity in large-scale MEA electrolyzers by efficiently tailoring the ionomeric binder.

1. Introduction

The electrochemical reduction of carbon dioxide (CO_2R) has been identified as a promising approach to compensate anthropogenic CO_2 emission, while generating high value chemicals and fuels.[1,2] CO_2R can be easily coupled with intermittent renewable electricity sources,[3] operating at ambient temperature (T) and pressure, therefore representing an attractive alternative to processes relaying on fossil feedstock.[4,5] In the last decade, researchers have mainly focused on a lab scale systems, adjusting catalyst,[6,7] membranes,[8,9] and reactor configuration[10] to improve mass transport and guide the selectivity of CO_2R toward single carbon products (C_1), such as carbon monoxide (CO) and formate, or multicarbon (C_{2+}) products like ethylene, ethanol, and propanol.[11–13]

At large scale, technoeconomic studies have shown that electrochemical CO_2R approach can be economically feasible.[14–16] However, to meet industrial benchmarks, the electrolyzers must achieve energy efficiency (EE) exceeding 50%, current densities (j) above 200 mA cm^{-2} and low cell potential (<3.0 V), while addressing operational obstacles associated to the cell size increasing.[17–19] In-plane pressure variation,[20] long-term stability,[21] separation of products,[22] and reactor design[23,24] limit the process viability leading to increased investment and process costs.[25,26]

Among the different products, the electrochemical reduction of CO_2 to CO results as the most industrially feasible approach, due to his high selectivity, large current densities, and simple separation of the gas product from the electrolyte.[27–29] To date, successful and selective examples of large-scale electrochemical CO_2R electrolyzers have been achieved using gas diffusion electrodes (GDEs) and zero-gap membrane electrode assembly (MEA) configuration.[30–32]

The use of a GDE enables a short gas-phase pathway to the catalyst surface, overcoming limitations related to CO_2 low solubility and mass transport in aqueous electrolytes.[33–35] In the zero-gap configuration, an ionic active polymer membrane is directly sandwiched between two catalytic active electrodes, while liquid electrolyte recirculates only through the porous anode, reducing Ohmic losses and cell resistance.[36,37]

Efficient and industrially relevant CO_2 to CO conversion rates have been achieved with this configuration employing anion exchange membranes (AEMs).[38–40] In fact, in AEM-based electrolyzers, the alkaline environment suppresses the competing hydrogen evolution reaction (HER).[41,42] However, a major challenge in

L. Gatti, S. Verhovez, A. Mezza, M. Etzi, C. F. Pirri, A. Sacco
Istituto Italiano di TecnologiaCenter for Sustainable Future Technologies Department @Polito
Via Livorno 60, 10144 Torino, Italy
E-mail: laura.gatti@polito.it; adriano.sacco@iit.it

L. Gatti, S. Verhovez, A. Mezza, S. Stassi, C. F. Pirri
Department of Applied Science and Technology
Politecnico di Torino
Corso Duca Degli Abruzzi 24, 10129 Torino, Italy

The ORCID identification number(s) for the author(s) of this article can be found under https://doi.org/10.1002/aesr.202500312.

DOI: 10.1002/aesr.202500312

these devices is the long-term stability, which is compromised by salt formation in the cathode chamber.

Under applied negative potentials, alkali metal cations (M^+) migrate from the anode to the cathode. The cations migration through the anionic membrane essentially enables[43,44] and accelerates[45] the CO_2RR, by stabilizing the reaction intermediates. However, at the cathode in a CO_2 and OH^- rich environment (Equation (1)), these hydrated cations react with carbonate and bicarbonate anions forming salt deposits (Equation (2)).

$$CO_2 + H_2O + 2e^- \rightarrow CO + 2OH^- \quad (1)$$

$$CO_2 + 2OH^- + 2M^+ \rightarrow M_2CO_3 + H_2O \quad (2)$$

Due the humidified and continuous gas flow, the salts slowly move from the membrane-cathode interface through the GDE precipitating to the back of the electrode and in the electrolyzer flow field.[46] The salt deposits progressively create pressure buildup and obstruct CO_2 access to the catalyst surface, ultimately leading to the promotion of HER and the electrolyzer failure.[47]

To mitigate this problem and increase long-term operation, several strategies have been proposed. Active strategies include periodic change in the operational state of the electrolyzer, while passive procedures have a continuous effect on the system.[48] In particular, Endrodi et al. have proposed a purge of water and solvent to rinse the deposits and reactivate the cathode. While performing intermitted cycle of cleaning and activation of the electrode, they were able to operate a deionized water-fed CO_2 electrolyzer for over 200 h working at $j = 420 \pm 50$ mA cm^{-2} and T= 60 °C.[49] However, later work from the same group questioned the rinsing procedure as a viable long-term solution, because effective cleaning within GDE structure requires the application of significance pressure, which may compromise the electrode integrity.[50,51]

Xu et al.[52] have reported employment of a periodic regeneration voltage to actively redistribute ions within the MEA, by alternating between operational steps at 3.8 V_{cell} and regenerative phases at 2.0 V_{cell}. Without a regenerative voltage, the electrolyzer fails after only 10 h due to salt formation, while 236 h were achieved with pulsed electrolysis. However, the industrial feasible employment is limited compared to static operation, due to decrease in production and increased cost.[53]

To passively mitigate salt accumulation, various operational parameters have been systematically evaluated and validated. Ramdin et al.[54] have investigated the effect of six different binding materials on the electrode stability. Their findings showed that when employing flood-resistant GDE the binder hydrophobicity is not essential for stable operation. However, the stability was only evaluated with short-term measurement (<200 min) and in 5 cm^2 electrolyzer. Several studies have attempted to quantify the migration of alkali cations over time in MEA systems. Considering the crucial roles of the alkali cations, Kamiya et al.[55] have conducted a quantitative evaluation to correlate the CO_2R activity with cations migration to improve the system stability. Cofell et al.[42] investigated the location and degree of salt precipitation for different anolytes, including various alkali cations, using post-mortem scanning electron microscopy of the GDE.

At a larger scale, Endrődi et al.[42] experimentally validated the effects of temperature and commercial AEMs on salt deposition. By optimizing these parameters, they reached more than 100 h of stable operation using a 100 cm^2 custom MEA cell. Similarly, Biemolt et al.[56] employed inductively coupled plasma (ICP) measurements to quantify the rate of cations accumulation at predefined operating times, thereby verifying the combined effects of the metal cation, anolyte concentration, temperature, and membrane properties. Their optimized configuration, which included high alkali soluble caesium cation (Cs^+) and T = 60 °C, enabled continuous cell operation of 144 h. However, among all the different operational parameters studied, the role of the binder has not been extensively investigated in large-scale electrolyzers.

In this work, we successfully scaled up a zero-gap MEA electrolyzer for CO production, from 5 cm^2 to 100 cm^2 under ambient conditions. To enable this transition, we systematically investigated the passive influence of various electrodes components in a 5 and 25 cm^2 electrolyzers. We optimized the loading of silver nanoparticles (NPs) and ionomeric binder to minimize initial costs and screened five different hydrophobic substrates, adjusting cell compression based on both substrate characteristics and electrolyzer size. The combined and optimized parameters were successfully validated in a 100 cm^2 cell.

To the best of our knowledge, for the first time we identified the ionomer binder as the critical element influencing both selectivity and electrode stability. Here, indeed we demonstrated a direct correlation between the binder performance and salt accumulations, thereby essentially affecting the electrode long-term stability. This work provides valuable tools to understand and tailor electrode components to mitigate salt accumulation and increase long-term stability in large-scale CO_2 electrolyzers.

2. Results and Discussion

Aiming to meet industrial benchmarks, initial optimization focused on enhancing the faradaic efficiency (FE) toward CO and reducing the cell overpotential at the laboratory scale using a 5 cm^2 commercial MEA electrolyzer.

The MEA cell was assembled by compressing a Sustainion x37-50 Grade-RT AEM between a silver-based GDE and a titanium felt coated with IrO_2 at a loading of 2.5 mg cm^{-2}. The cathode GDEs were prepared by automatically spray coating an optimized ink dispersion containing Ag NPs (Figure S1, Supporting Information) onto commercially available gas diffusion layer (GDL) carbon papers. The anode was prepared adopting either dip-coating or spray coating techniques depending on the electrolyzer size, to achieve homogeneous deposition (Figure S2–S3, Supporting Information). During operation, humidified CO_2 was fed to the cathode, while 0.1 M $CsHCO_3$ anolyte was continuously recirculated through the anode.

The investigation primarily targeted the cell main components, especially the cathode manufacturing, which offers most degrees of freedom for performance improvements. As reported in **Figure 1**, progressive variation of the Ag NPs loading from 0.5 mg cm^{-2} to 1.5 mg cm^{-2} showed negligible change of the FE_{CO} which remained consistently over 90% at a current density of 300 mA cm^{-2} during chronopotentiometry (CP) measurements. Given this result, the low loaded catalyst was selected among other samples to facilitate a future scale-up, aiming to reduce initial costs related to the amount of catalyst employed.[57]

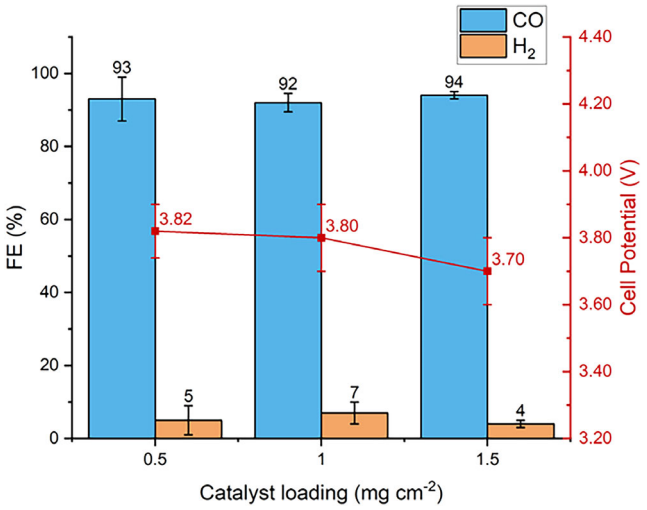

Figure 1. FEs for CO and H_2 (bars, left axis) and cell potential (red points, right axis) recorded with CP measurements at $j = 300$ mA cm^{-2}, employing silver-based cathodes with increasing catalyst loading. 0.1 M $CsHCO_3$ was employed as the anolyte.

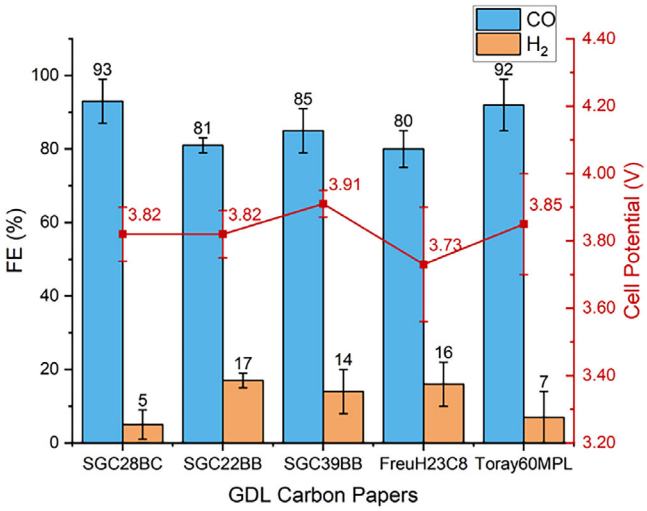

Figure 3. FEs (bars, left axis) and cell potential (red points, right axis) obtained from CP measurements at $j = 300$ mA cm^{-2} using different commercial carbon papers as substrates. 0.1 M $CsHCO_3$ was employed as the anolyte.

After selecting the minimal catalyst loading, a systematic screening of various substrates was performed. Five different commercial GDL carbon papers (Sigracet 28BC, Sigracet 39BB, Sigracet 22BB, Toray 60-MPL and Freudenberg H23C8) were selected and electrochemically tested. To ensure controlled and optimal compression, the cells were assembled accordingly to the substrate's thicknesses. The compression ratio was optimized for each GDLs separately, starting with the gasket spacing matching the total thickness of the cathode GDE, and the electrochemical response was evaluated while gradually lowering the cathode gasket thickness (Figure S4, Supporting Information). Field emission scanning electron microscopy (FESEM) images (**Figure 2**a–j) of the commercially available substrates were used to reveal other characteristics, including surface cracking and carbon fiber layers (CFLs) morphology which, as shown later, would have an impact on the electrochemical performance (Table S1, Supporting Information). However, all chosen substrates contain a hydrophobic agent in the microporous layer (MPL), where the effect of the polymer in the GDL has been studied and proven as fundamental elements to improving the cell durability and efficiency.[58,59]

The electrochemical results in **Figure 3** showed that the Sigracet 28BC and Toray60MPL exhibited the best performance, maintaining FE_{CO} steadily over 90%. Although the Sigracet 39BB and 22BB also share straight-like carbon fiber arrangement, their performances were significantly different compared to the best performing substrates. This discrepancy is probably due to their difference in porous structure and morphology of the surface cracking, which highly influence other crucial properties like the wettability and cell resistance.[60] The Freudenberg H23C8 showed subpar performance compared with the others, which may be correlated to its different surface morphology and spaghetti-like fiber structure, which may affect the GDL's wetting properties.[61] Slight variation was found in the cell overpotential, with the thicker GDLs (i.e., SGC39BB and Toray60MPL) generally leading to higher cell voltage. Electrochemical impedance spectroscopy (EIS) analysis reported in Table S2, Supporting Information, and based on methodical experimental data (Figure S5, Supporting Information) showed that electrodes with comparable thicknesses, e.g., the SGC22BB and SGC28BC, exhibited lower charge-transfer resistance when higher porosity and surface cracking were present, implying better CO_2R performance.[42,62] Furthermore, when

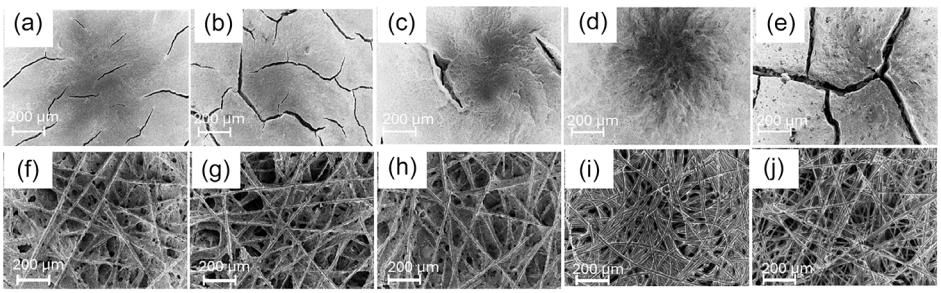

Figure 2. FESEM images of a–e) MPL and f–j) CFL sides of GDEs prepared by spray coating Ag NPs (0.5 mg cm^{-2}) onto five different commercial carbon papers: (a,f) SGC28BC, (b,g) SGC22BB, (c,h) SGC39BB, (d,i) FreuH23C8, and (e,j) Toray60MPL. The images represent multiple samples and reflect consistent morphology within each type of GDL.

comparing electrodes with similar charge transfer resistance but different carbon fiber morphologies, e.g., the SGC28BC (straight fiber) and FreuH23C8 (spaghetti-like fiber), the former exhibits higher double layer capacitance, indicating greater number of active sites.[63,64] This suggests that, even at comparable charge-transfer resistance, the straight fiber morphology enhances the accessibility of active sites, improved selectivity and overall performance.

As a result, the SGC28BC was selected among the others as it exhibited the best trade-off, leading to both high FE_{CO} and lower cell potential, which are the crucial performances needed to achieve feasible scaling up of the CO_2 electrolyzer.

Another fundamental component affecting the electrode activity is the polymeric binder, which not only provides catalyst adhesion[30] but also facilitates ions transport,[65] modulating the local pH on the catalyst surface and creating a favorable microenvironment for CO_2R. As presented in **Figure 4**a, four commercially available ionomer binders were selected: Sustainion XA-9, PiperION, Fumion FAA-3-SOLUT-10 and Nafion-117 dispersions. Initially, the various binders were tested in equal percentage (5% in relation to the amount of catalyst weight) to primarily evaluate and correlate the effect of their chemical structure and charge to the electrochemical performance.[66]

The Nafion-117 is the only cation exchanging ionomer, composed by a Teflon backbone functionalized with sulfonic group. However, due to its limited OH^- ions transport properties, it exhibits subpar performance compared to the other binders.[67] Systematic EIS measurements (Table S3 and Figure S6, Supporting Information) confirm this performance: Nafion-117 exhibits a lower double-layer capacitance, whereas the other ionomer binders show no significant differences.

All the other binders are anion exchange ionomers. In particular, Fumion FAA-3 has a polyaromatic backbone with quaternary ammonium functional groups, based on a proprietary hydrocarbon resin. While the best performing dispersions, Sustainion and PiperION, present a rigid aryl backbone, respectively, with an alkaline stable piperidinium group and an imidazolium-group. Nitrogen is a characteristic element in the functional groups of anion exchange binder as it stabilizes the reaction interacting with CO_2 and stabilizing CO_2RR intermediates.[68] Their proprietary backbone structure and functional

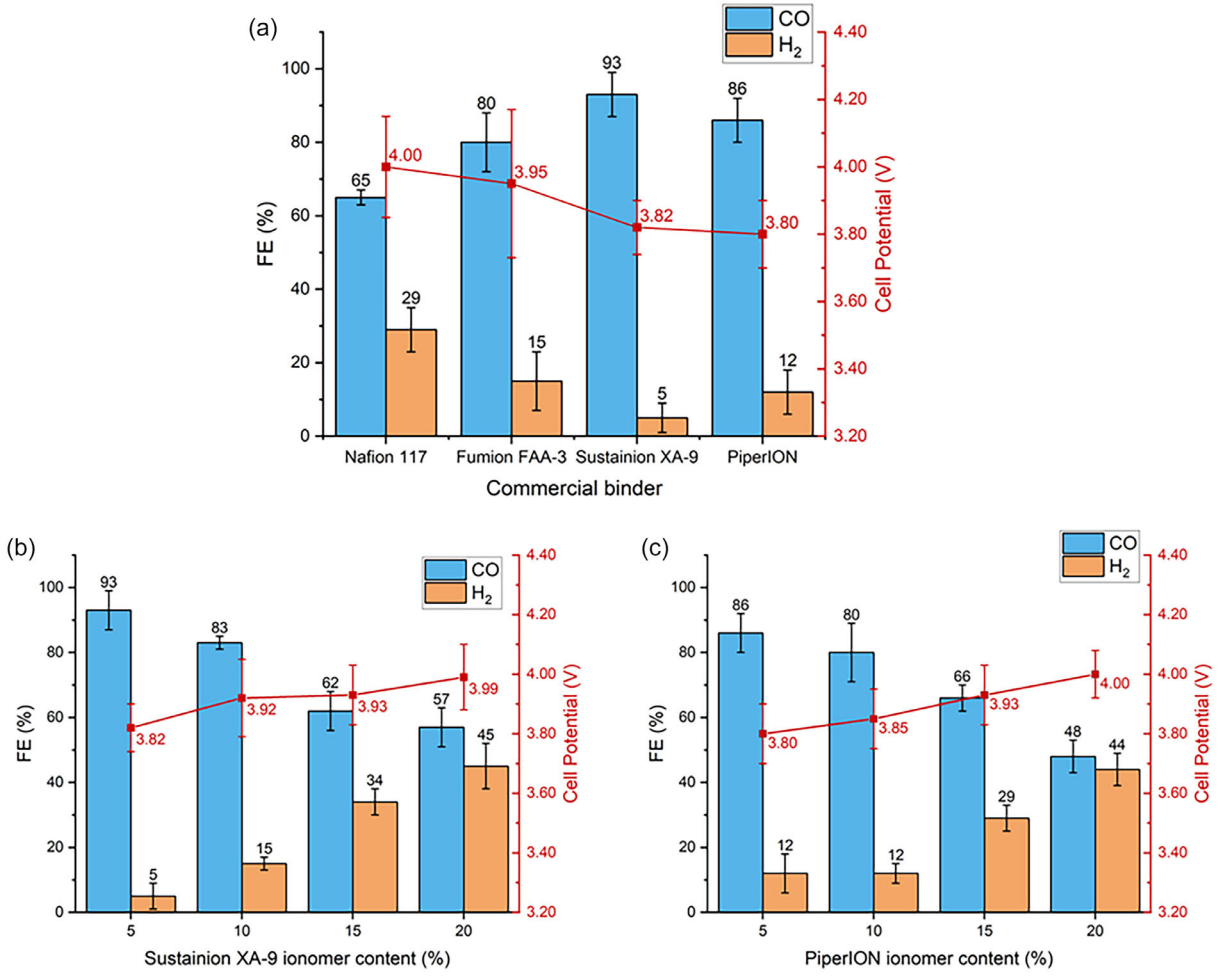

Figure 4. Cell potential (red points, right axis) and FEs (bars, left axis) obtained from CP measurements at $j = 300$ mA cm^{-2} of a) GDEs prepared with various polymeric binders at a fixed catalyst to binder ratio (5% cat. wt.). b) Sustainion XA-9 and c) PiperION -based GDEs tested increasing the content of ionomers added in the dispersion ink, from 5% to 20% cat. weight. In all measurements, 0.1 M $CsHCO_3$ was employed as the anolyte.

group significantly affect the ionic conductivity and the overall cell performance.[69]

The two best performing ionomers, Sustainion and PiperION, were further investigated to define the optimal amount of binder that enables the highest catalyst activity. In Figure 4b,c, a clear trend emerged: increasing binder content led to progressively higher cell resistance and overpotential, as well as lower FE_{CO} in agreement with previous literature.[70] This effect was particularly pronounced when increasing from 10% to 15% catalyst weight (cat. wt.), which resulted in a progressive decline in performance. An increased binder content typically reduces the electrode conductivity due to limited electron transfer and simultaneously decreases the availability of active sites.[71] As a results, the 5% cat. wt. of ionomer binders emerges as the optimal amount considering the component cost, reduced conductivity, and activity of the electrodes.

To further investigate the effect of the ionomer binder on salt accumulation, caesium distribution maps were performed employing energy-dispersive X-ray (EDX) Spectroscopy. **Figure 5** presents the cross-sectional EDX maps illustrating the Cs accumulation in the spent electrodes prepared with the different ionomers (5% cat. wt.), after 1 h of operation (to provide additional context, Figure S7, Supporting Information presents, the distribution of the Ag catalyst onto the electrodes). All electrodes maintained stable FEs throughout this period (Figure S8, Supporting Information). However, the Nafion-117 and Fumion FAA-3-SOLUT-10 samples, which exhibited the lowest selectivity, also showed a greater accumulation of Cs salts.[50]

On the other hand, the electrodes with higher and comparable selectivity toward CO, i.e., PiperION and Sustainion, displayed significantly salt deposition. This suggests that low CO_2R selectivity, increases the competitive HER which promotes salt formation, as unreacted CO_2 remains available for carbonation reactions, thereby reducing the stability of the electrolyzer.[56,72]

The short-term 1 h electrochemical measurement showed a comparable selectivity between the PiperION- and Sustainion-based GDEs. However, the Cs mapping demonstrated a minor Cs concentration in the PiperION-based electrode. To further validate a possible correlation between ionomer type and cations accumulation, we conducted long-term electrochemical measurements up to failure at industrially relevant current density ($j = 300\ mA\ cm^{-2}$).

Before doing this, we increased the scale of the reactor, moving toward the real-world application, and tested the optimized recipe for electrode production first in a $25\ cm^2$ reactor and then in a $100\ cm^2$ reactor. As shown in Figure S9, Supporting Information, increasing the reactor size, it was necessary to progressively increase the total cell compression, until proper electrical contact was reach. Nevertheless, as exhibited in Figure S10, Supporting Information, scaling up the electrolyzer size, the overall cell performances were kept stable at all investigated current densities (100 to $300\ mA\ cm^{-2}$).

Therefore, to exclusively validate the role of ionomer, electrodes for long-term operations were prepared with equal catalyst loading, substrate, cell compression, and amount of ionomer binder and operated with identical parameters.

As showed in **Figure 6** and Figure S11, Supporting Information, the continuous operation clearly confirms a more stable performance with the PiperION electrode. After only 20 h of

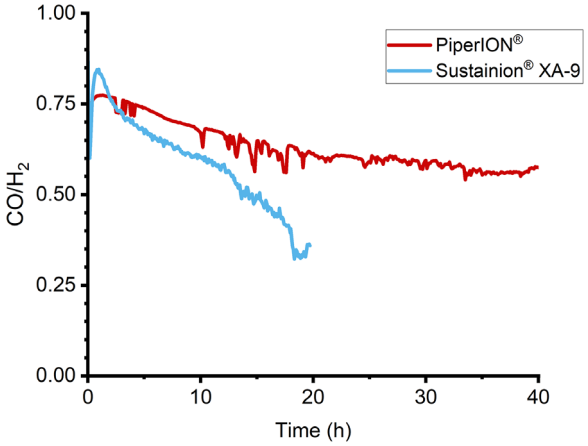

Figure 6. CO to H_2 production ratio during CP measurements ($j = 300\ mA\ cm^{-2}$) in a $100\ cm^2$ cell, employing 5% cat. wt. Sustainion XA-9 (blue) and PiperION (red)-based GDEs. The anolyte solution employed is 0.1 M $CsHCO_3$ with flow rate of $100\ mL\ min^{-1}$, humidified CO_2 fed to the cathode with a flow rate of $420\ mL\ min^{-1}$, at room temperature and pressure.

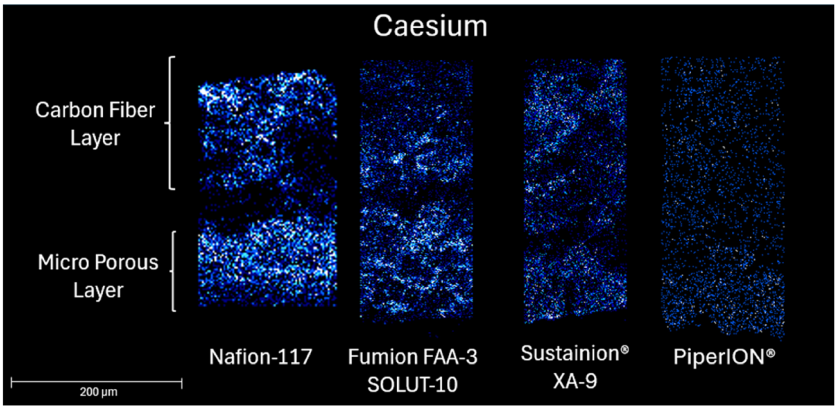

Figure 5. Cross-sectional SEM-EDX images showing Cs distribution in GDEs with different types of ionomer binders (5% cat. wt.), after 1-h CP measurements ($j = 300\ mA\ cm^{-2}$). 0.1 M $CsHCO_3$ was employed as the anolyte.

operation, the Sustainion-GDE experienced a 60% decrease in FE_{CO}, while the PiperION-containing electrode exhibited only a 20% reduction in efficiency for 40 h of operation. The use of the PiperION binder resulted in a minimum 100% improvement in stability, doubling the operational time from 20 to 40 h, without failure.

These results may validate the hypothesis of a direct correlation between the binder's properties, salt accumulation and consequently electrode degradation. Initially, in short-term experiments the ionomer's chemical structure provides good and comparable ionic conductivity for both the Sustainion- and PiperION-based electrodes.[42] However, during extended electrochemical operation the polymer stability may significantly decrease due to possible nucleophilic substitution and ring-opening reactions affecting the functional groups.[65,73–75] The six-membered piperidinium rings are more sterically protected and chemically stable than the imidazolium rings, making PiperION more resistant to degradation. The ionomers degradation may reduce the CO_2R performance and lead to salt formation and cell failure.[76,77]

This association between the ionomer role and cell stability is further validated by the cross-sectional SEM-EDX images that show the Cs distribution in the spent anionic binder-based electrodes after 20 and 40 h of operation at a current density of 300 mA cm^{-2} in a 100 cm^2 electrolyzer. As shown in **Figure 7**, despite the shorter operational period, the 20-h Sustainion-based GDE still exhibits a significantly higher accumulation of Cs deposits (Figure S12, Supporting Information) compared with the 40-h PiperION-based electrode, while in short-term experiments, the ionomer-based electrodes exhibited comparable selectivity; over longer operation, the ionomeric binder substantially impacts the stability.[78]

Collectively, these results provide evidence that the polymeric binder can significantly influence CO_2 selectivity through its backbone structure and functional groups.[79] However, we also proved that the choice of binder can profoundly affect cation accumulation, promoting salt deposition, thereby compromising the long-term stability of the electrolyzer.

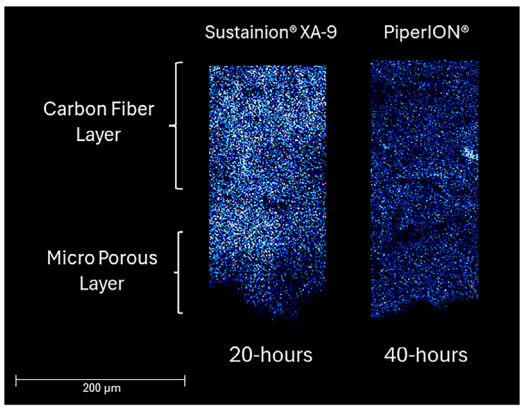

Figure 7. Cross-sectional SEM-EDX images showing Cs distribution in 5% cat. wt. Sustainion XA-9 and PiperION based GDEs (5% cat. wt.), after 20- and 40-h CP measurements (j = 300 mA cm^{-2}) in a 100 cm^2 electrolyzer. The anolyte solution employed is 0.1 M $CsHCO_3$ with flow rate of 100 mL min^{-1}, and humidified CO_2 fed to the cathode with a flow rate of mL min^{-1}.

3. Conclusion

In this study, we successfully performed an initial scale-up of a commercial zero-gap MEA electrolyzer from 5 cm^2 to 100 cm^2, maintaining high performance under ambient temperature and pressure conditions. A systematic investigation was conducted on key electrode components as catalyst loading, GDL substrates, cell compression, content, and binder types while increasing the electrolyzer active area. We identified and optimized the critical parameters influencing the electrochemical reduction of CO_2 to CO, to reach on a larger scale FE_{CO} >90% at industrially relevant current density of 300 mA cm^{-2}.

Through this analytical approach, we further demonstrated the crucial role of polymeric binders, not only affecting selectivity but, more importantly, in determining long-term operational stability. In a 100 cm^2 electrolyzer, under identical operating conditions, the PiperION$^+$-based electrode maintained stable CO selectivity for up to 40 h, experiencing only a 20% decline in FE_{CO}. In contrast, the Sustainion-based GDE exhibited a 60% drop in selectivity after just 20 h. These findings were supported by Cs distribution mapping, during short and long-term operation, which confirmed a lower Cs accumulation in the PiperION-based electrodes.

Overall, the results highlight a direct correlation between the binder structure and electrode degradation, indicating that improper ionomer selection can essentially accelerate cell failure via salt precipitation. Collectively, this work provides detailed insights into how to passively mitigate the salt formation and cell failure in large scale MEA electrolyzer by effectively tailoring the electrode components. These findings underscore the crucial importance of a complete and continuous evaluation of the electrode components during long-term operation, to fully comprehend their influence on performance and durability. Future research should aim to adapt this knowledge to noncommercial catalysts to further support their implementation in larger scale CO_2 electrolyzers.

Supporting Information

Supporting Information is available from the Wiley Online Library or from the author.

Acknowledgements

This publication is part of the project PNRR-NGEU which has received funding from the MUR – DM 118/2023 and 630/2024. In addition, funding from EU's Horizon 2021 programme under the Marie Skłodowska-Curie Doctoral Networks (MSCA-DN) (grant agreement no. 101072830) (ECOMATES) is acknowledged. Finally, this study was partially developed in the framework of the research activities carried out within the Project "Network 4 Energy Sustainable Transition—NEST," Spoke 4, Project code PE0000021, funded under the National Recovery and Resilience Plan (NRRP), Mission 4, Component 2, Investment 1.3—Call for tender No. 1561 of 11.10.2022 of Ministero dell'Università e della Ricerca (MUR); funded by the European Union—NextGenerationEU.

Conflict of Interest

The authors declare no conflict of interest.

Data Availability Statement

The data that support the findings of this study are available from the corresponding author upon reasonable request.

Keywords

alkaline electrolyzers, CO_2 reduction reaction, membrane electrode assembly, salt formation, scale-up

Received: August 31, 2025
Published online:

[1] S. Overa, B. H. Ko, Y. Zhao, F. Jiao, *Acc. Chem. Res.* **2022**, *55*, 638.
[2] C. Chen, J. F. K. Kotyk, S. W. Sheehan, *Chemistry* **2018**, *4*, 2571.
[3] M. Agliuzza, A. Mezza, A. Sacco, *Appl. Energy.* **2023**, *334*, 120649.
[4] P. De Luna, C. Hahn, D. Higgins, S. A. Jaffer, T. F. Jaramillo, E. H. Sargent, *Science* **2019**, *364*, 6438.
[5] R. Baños, F. Manzano-Agugliaro, F. G. Montoya, C. Gil, A. Alcayde, J. Gómez, *Renew. Sustain. Energy Rev.* **2011**, *15*, 1753.
[6] D. Gao, R. M. Arán -Ais, H. S. Jeon, B. R. Cuenya, *Am. Chem. Soc.* **2024**, *146*, 15917.
[7] A. Bagger, J. Wen, A. S. Varela, P. Strasser, J. Rossmeis, *Chem. Phys. Chem.* **2017**, *18*, 3266.
[8] F. Habibzadeh, P. Mardle, N. Zhao, H. D. Riley, D. A. Salvatore, C. P. Berlinguette, S. Holdcroft, Z. Shi, *Electrochem. Energy Rev.* **2023**, *6*, 26.
[9] H. Rabiee, P. Yan, H. Wang, Z. Zhu, L. Ge, *EcoEnergy.* **2024**, *2*, 3.
[10] D. Gao, P. Wei, H. Li, L. Lin, G. Wang, X. Bao, *Acta Phys. -Chim. Sin.* **2021**, *37*, 2009021.
[11] J. K. Dangbegnon, M. Etzi, J. Zeng, A. Chiodoni, C. F. Pirri, *Catal. Sci. Technol.* **2025**, *15*, 2318.
[12] A. Huang, J. Yu, J. Zhang, Y. Zhang, Y. Wu, Y. Wang, W. Luo, *Catalysts.* **2025**, *15*, 199.
[13] X. Wang, P. Ou, A. Ozden, S.-F. Hung, J. Tam, C. M. Gabardo, J. Y. Howe, J. Sisler, K. Bertens, F. Pelayo García de Arquer, R. K. Miao, C. P. O'Brien, Z. Wang, J. Abed, A. S. Rasouli, M. Sun, A. H. Ip, D. Sinton, E. H. Sargent, *Nat. Energy.* **2022**, *7*, 170.
[14] S. Verma, B. Kim, H.-R. Jhong, S. Ma, P. J. A. Kenis, *Chem. Sus. Chem.* **2016**, *9*, 1972.
[15] J. Na, B. Seo, J. Kim, C. W. Lee, H. Lee, Y. J. Hwang, B. K. Min, D. K. Lee, H.-S. Oh, U. Lee, *Nat Comm.* **2019**, *10*, 5193.
[16] P. Ganji, R. A. Borse, J. Xie, A. G. A. Mohamed, Y. Wang, *Adv. Sustain.Syst.* **2020**, *4*, 2000096.
[17] G. Kibria, J. P. Edwards, C. M. Gabardo, C. Dinh, A. Seifitokaldani, D. Sinton, E. H. Sargent, *Adv. Mater.* **2019**, *31*, 1807166.
[18] H. Shin, K. U. Hansen, F. Jìao, *Nat. Sustain.* **2021**, *4*, 911.
[19] D. Segets, C. Andronescu, U. Apfel, *Nat. Commun.* **2023**, *14*, 7950.
[20] V. E. Nelson, C. P. O'Brien, J. P. Edwards, S. Liu, C. M. Gabardo, E. H. Sargent, D. Sinton, *ACS Appl. Mater. Interfaces* **2024**, *16*, 50818.
[21] W. Lai, Y. Qiao, Y. Wang, H. Huang, *Adv. Mater.* **2023**, *35*, 2306288.
[22] M. Ramdin, A. R. T. Morrison, M. De Groen, R. Van Haperen, R. De Kler, E. Irtem, A. Laitinen, L. Van Den Broeke, T. Breugelmans, J. Trusler, W. Jong, T. Vlugt, *Ind. Eng. Chem. Res.* **2019**, *58*, 22718.
[23] D. G. Wheeler, B. A. W. Mowbray, A. Reyes, F. Habibzadeh, J. He, C. P. Berlinguette, *Energy Environ. Sci.* **2020**, *13*, 5126.
[24] Y. Yang, F. Li, *Curr. Opin. Green Sustain. Chem.* **2021**, *27*, 100419.
[25] J. W. Sun, H. Q. Fu, P. F. Liu, A. Chen, P. Liu, H. G. Yang, H. Zhao, *EES Catal.* **2023**, *1*, 934.
[26] B. Belsa, L. Xia, F. Pelayo García de Arquer, *ACS Energy Lett.* **2024**, *9*, 4293.
[27] R. Krause, D. Reinisch, C. Reller, H. Eckert, D. Hartmann, D. Taroata, K. Wiesner-Fleischer, A. Bulan, A. Lueken, G. Schmid, *Chem. Ing. Tech.* **2020**, *92*, 53.
[28] J. P. Edwards, T. Alerte, C. P. O'Brien, C. M. Gabardo, S. Liu, J. Wicks, A. Gaona, J. Abed, Y. C. Xiao, D. Young, A. S. Rasouli, A. Sarkar, S. A. Jaffer, H. L. MacLean, E. H. Sargent, D. Sinton, *ACS Energy Lett.* **2023**, *8*, 2576.
[29] A. Raya-Imbernón, A. A. Samu, S. Barwe, G. Cusati, T. Födi, B. M. Hepp, C. Janáky,, *ACS Energy Lett.* **2024**, *9*, 288.
[30] B. Endrődi, G. Bencsik, F. Darvas, R. Jones, K. Rajeshwar, C. Janáky, *Prog. Energy Combust. Sci.* **2017**, *62*, 133.
[31] L. Ge, H. Rabiee, M. Li, S. Subramanian, Y. Zheng, J. H. Lee, T. Burdyny, H. Wang, *Chem.* **2022**, *8*, 663.
[32] X. Wang, S. Zhao, T. Guo, L. Yang, Q. Zhao, Y. Wu, Y. Chen, *Trans. Tianjin Univ.* **2024**, *30*, 117.
[33] T. Burdyny, W. A. Smith, *Energy Environ. Sci.* **2019**, *12*, 1442.
[34] E. W. Lees, B. A. Mowbray, F. G. L. Parlane, C. P. Berlinguette, *Nat. Rev. Mater.* **2022**, *7*, 55.
[35] D. Wakerley, S. Lamaison, J. Wicks, A. Clemens, J. Feaster, D. Corral, S. A. Jaffer, A. Sarkar, M. Fontecave, E. B. Duoss, S. Baker, E. H. Sargent, T. F. Jaramillo, C. Hahn, *Nat. Energy* **2022**, *7*, 130.
[36] Z. Zhang, X. Huang, Z. Chen, J. Zhu, B. Endrődi, C. Janáky, D. Deng, *Angew. Chem.* **2023**, *62*, e202302789.
[37] O. Romiluyi, N. Danilovic, A. T. Bell, A. Z. Weber, *Electrochem. Sci. Adv.* **2023**, *3*, e2100186.
[38] S. Garg, C. A. Giron Rodriguez, T. E. Rufford, J. R. Varcoe, B. Seger, *Energy Environ. Sci.* **2022**, *15*, 4440.
[39] C. M. Gabardo, A. Seifitokaldani, J. P. Edwards, C.-T. Dinh, T. Burdyny, M. G. Kibria, C. P. O'Brien, E. H. Sargent, D. Sinton, *Energy Environ. Sci.* **2018**, *11*, 2531.
[40] T. Zheng, K. Jiang, N. Ta, Y. Hu, J. Zeng, J. Liu, H. Wang, *Joule* **2019**, *3*, 265.
[41] S. S. Bhargava, F. Proietto, D. Azmoodeh, E. R. Cofell, D. A. Henckel, S. Verma, C. J. Brooks, A. A. Gewirth, P. J. A. Kenis, *Chem. Electro. Chem.* **2020**, *7*, 2001.
[42] E. R. Cofell, U. O. Nwabara, S. S. Bhargava, D. E. Henckel, P. J. A. Kenis, *ACS Appl. Mater. Interfaces* **2021**, *13*, 15132.
[43] M. C. O. Monteiro, F. Dattila, B. Hagedoorn, R. García-Muelas, N. M. T. LópezKoper, M. T. Koper, *Nature Cat.* **2021**, *4*, 654.
[44] G. Marcandalli, M. C. O. Monteiro, A. Goyal, M. T. M. Koper, *Acc. Chem. Res.* **2022**, *55*, 1900.
[45] J. Resasco, L. D. Chen, E. Clark, C. Tsai, C. Hahn, T. F. Jaramillo, K. Chan, A. T. Bell, *J. Am. Chem. Soc.* **2017**, *139*, 11277.
[46] S. Hao, A. Elgazzar, N. Ravi, T.-U. Wi, P. Zhu, Y. Feng, Y. Xia, F.-Y. Chen, X. Shan, H. Wang, *Nat. Comm.* **2025**, 266.
[47] J. Disch, L. Bohn, S. Kock, M. Schulz, Y. Han, A. Tengattini, L. Helfen, M. Breitwieser, S. Vierrath, *Nat. Comm.* **2022**, *13*, 6099.
[48] M. Sassenburg, M. Kelly, S. Subramanian, W. A. Smith, T. Burdyny, *ACS Energy Lett.* **2023**, *8*, 321.
[49] B. Endrődi, E. Kecsenovity, A. Samu, F. Darvas, R. V. Jones, V. Török, A. Danyi, C. Janáky, *ACS Energy Lett.* **2019**, *4*, 1770.
[50] B. Endrődi, A. Samu, E. Kecsenovity, T. Halmágyi, D. Sebök, C. Janáky, *Nat. Energy.* **2021**, *6*, 439.
[51] L. M. Baumgartner, C. I. Koopman, A. Forner-Cuenca, D. A. Vermaas, *ACS Sustain. Chem. Eng.* **2022**, *10*, 4683.
[52] Y. Xu, J. P. Edwards, S. Liu, R. K. Miao, J. E. Huang, C. M. Gabardo, C. P. O'Brien, J. Li, E. H. Sargent, D. Sinton, *ACS Energy Lett.* **2021**, *6*, 809.
[53] Y. L. Chung, S. Kim, Y. Lee, D. T. Wijaya, C. W. Lee, K. Jin, J. Na, *iScience* **2024**, *27*, 110383.
[54] P. Gonugunta, K. Roohi, M. Soleimani, P. R. Anusuyadevi, P. Taheri, M. Ramdin, *Ind. Eng. Chem. Res.* **2025**, *64*, 2113.
[55] S. Kato, S. Ito, S. Nakahata, R. Kurihara, T. Harada, S. Nakanishi, K. Kamiya, *ChemSusChem.* **2024**, *17*, 202401013.

[56] B. Endrődi, E. Kecsenovity, A. Samu, T. Halmágyi, S. Rojas-Carbonell, L. Wang, Y. Yan, C. Janáky, *Energy Environ. Sci.* **2020**, *13*, 4098.
[57] J. Biemolt, J. Singh, G. Prats Vergel, H. M. Pelzer, T. Burdyny, *ACS Energy Lett.* **2025**, *10*, 807.
[58] J. W. Blake, J. W. Haverkort, J. T. Padding, *Electrochem. Acta* **2024**, *507*, 145177.
[59] Y. Wu, L. Charlesworth, I. Maglaya, M. N. Idros, M. Li, T. Burdyny, G. Wang, T. E. Rufford, *ACS Energy Lett.* **2022**, *7*, 2884.
[60] S. Hernandez-Aldave, E. Andreoli, *Catalysts.* **2020**, *10*, 713.
[61] A. A. Samu, I. Szenti, A. Kukovecz, B. Endrődi, C. Janáky, *Comm. Chem.* **2023**, *6*, 41.
[62] M. Etzi, J. Danghegnon, A. Chiodoni, C. F. Pirri, *J. CO2 Util.* **2024**, *83*, 102772.
[63] A. Sacco, *J CO2 Util.* **2018**, *27*, 22.
[64] H. Warkentin, C. P. O'Brien, S. Holowka, B. Maxwell, M. Awara, M. Bouman, A. S. Zeraati, R. Nicholas, A. H. Ip, E. S. Elsahwi, C. M. Gabardo, D. Sinton, *ChemSusChem* **2023**, *16*, 202300657.
[65] J. Zeng, M. Castellino, K. Bejtka, A. Sacco, G. Di Martino, M. A. Farkhondehfal, A. Chiodoni, S. Hernández, C. F. Pirri, *J Mater Sci.* **2021**, *56*, 1255.
[66] S. Favero, I. E. L. Stephens, M.-M. Titirci, *Adv. Mater.* **2024**, *36*, 2308238J.
[67] R. A. Tufa, D. Chanda, M. Ma, D. Aili, T. B. Demissie, J. Vaes, Q. Li, S. Liu, D. Pant, *Appl. Energy* **2020**, *277*, 11555.
[68] U. O. Nwabara, A. D. Hernandez, D. A. Henckel, X. Chen, E. R. Cofell, M. P. de-Heer, S. Verma, A. A. Gewirth, P. J. A. Kenis, *ACS Appl. Energy Mater.* **2021**, *4*, 5175.
[69] L. Yang, X. Lv, C. Peng, S. Kong, F. Huang, Y. Tang, L. Zhang, G. Zheng, *ACS Cent. Sci.* **2023**, *9*, 1905.
[70] H. Lee, S. Kattel, Z. Xie, B. M. Tackett, J. Wang, C.-J. Liu, J. G. Chen, *Adv. Funct. Mater.* **2018**, *28*, 1804762.
[71] Z. Xing, L. Hu, D. S. Ripatti, X. Hu, X. Feng, *Nat. Commun.* **2021**, *12*, 136.
[72] J. A. Abarca, G. Diaz-Sainz, A. Irabien, *J CO2 Util.* **2024**, *86*, 102897.
[73] O. Romiluyi, N. Danilovic, A. T. Bell, A. Z. Weber, *Electrochem. Sci. Adv.* **2023**, *3*, 2100186.
[74] N. Chen, Y. Jin, H. Liu, C. Hu, B. Wu, S. Xu, H. Li, J. Fan, Y. M. Lee, *Angew. Chem. Int.* **2021**, *60*, 19272.
[75] R. A. Krivina, G. A. Lindquist, M. C. Yang, A. K. Cook, C. H. Hendon, A. R. Motz, C. Capuano, K. E. Ayers, J. E. Hutchison, S. W. Boettcher, *ACS Appl. Mater. Interfaces* **2022**, *14*, 18261.
[76] Y. Chen, T. Lei, L. Xu, C. Jin, J. Yi, S. Liu, S. Lin, Y. Yang, H. Song, K. Wang, H. Fan, C. Zheng, X. Zhang, X. Gao, *J. Mater. Chem. A.* **2024**, *12*, 17181.
[77] N. Chen, Y. N. Lee, *Prog. Polym. Sci.* **2021**, *113*, 101345.
[78] Q. Li, M. Hu, C. Ge, Y. Yang, L. Xiao, L. Zhuang, H. D. Abruna, *Chem. Sci.* **2023**, *14*, 10429.
[79] Y. Chae, H. Kim, D. K. Lee, D. H. Won, *Nano Energy* **2024**, *130*, 110134.